PAPER

Check for updates

Bio-response of copper–magnesium co-substituted mesoporous bioactive glass for bone tissue regeneration

Akrity Anand,[ab] Hana Kaňková,[a] Zuzana Hájovská, [c] Dušan Galusek,[a] Aldo R. Boccaccini*[b] and Dagmar Galusková *[a]

Mesoporous bioactive glass (MBG) is widely acknowledged in bone tissue engineering due to its mesoporous structure, large surface area, and bioactivity. Recent research indicates that introduction of metallic ions has beneficial impacts on bone metabolism and angiogenesis. Thus, the features of MBG can be modified by incorporating combinations of ions, such as magnesium (Mg) and copper (Cu), which can play a considerable role in bone formation, influencing angiogenesis, osteogenesis, as well as antibacterial properties. In this study, Mg and Cu were co-doped for the first time (in a ratio of 1:1) in $80SiO_2–5P_2O_5–(15 − 2x)CaO–xMgO–xCuO$ glass composition with x = 0, 0.5, 1, and 2 mol%, synthesized using the sol–gel and evaporation-induced self-assembly method. X-ray diffraction analysis confirmed the amorphous nature of the powders, while inductively coupled plasma-optical emission spectrometry verified the existence of dopant ions in the respective amounts. The nitrogen sorption method indicated the formation of uniform cylindrical mesopores which are open at both ends and a high surface area of the powders. TEM images show fringes, indicating an ordered mesoporous structure in all MgCu co-doped systems. *In vitro* bioactivity was observed in all MBG powders, confirmed by the formation of an apatite phase when placed in simulated body fluid (SBF). Flake-like microstructure characteristics of HAp crystals found on the surface of MBG powders were visualized using FESEM. Cytotoxicity tests at lower concentrations (0.1 and 1 wt/vol%) of co-doped 2MC MBG (co-doping up to 2 mol%) showed cell proliferation and viability of osteoblast-like MG-63 cells and normal human dermal fibroblast (NHDF) cells similar to the basic glass 80S. Antibacterial study of MBG pellets showed an increment in the zone of inhibition with the sequential addition of doping ions. The turbidity measurement of bacterial cultures revealed that the optimal concentration for effectively inhibiting bacterial growth was 1 wt/vol% (*i.e.*, 10 mg mL^{-1}) concentration of MBG extracts. The result suggested that the incorporation of Mg and Cu ions in MBG in lower concentrations of up to 2 mol% can be useful in bone regeneration owing to bioactivity, cell proliferation, and antibacterial characteristics.

1. Introduction

In bone biology, phosphorus (P) and calcium (Ca) are the most important inorganic components of the mineralized matrix. Around 99% of Ca and 85% of P (in orthophosphate form $PO_4{}^{3-}$) are present in the bone matrix, which are complexed together to form hydroxyapatite (HAp), widely known as the bone mineral.[1,2]

Human bones also contain several other ions, which promote constructive metabolism in osseous tissues. As an example, a large amount of zinc (Zn) is present on haversian surfaces of bone, and its absence impairs skeletal development.[3] Magnesium (Mg) is required for several enzymatic reactions ranging from energy metabolism to nucleic acid and protein production. Its deficiency may lead to malabsorption syndrome, renal dysfunction, and hormonal imbalance.[4] Strontium (Sr) is widely considered for the cure of osteoporosis in the form of strontium ranelate tablets.[5] Similarly, copper (Cu) ions are known to stimulate endothelial cells to initiate angiogenesis. Besides Ca and P, Zn, Mg, Sr, and Cu are also considered biologically active ions, playing an important role in osseous tissue formation, stimulating its regeneration.

HAp, as the major mineral phase of bone, can develop direct bonds with bioactive glasses.[6] Mesoporous bioactive glasses

[a] Centre for Functional and Surface Functionalized Glass, TnUAD, 911 01 Trenčín, Slovakia. E-mail: dagmar.galuskova@tnuni.sk

[b] Institute of Biomaterials, University of Erlangen-Nuremberg, 91058 Erlangen, Germany. E-mail: aldo.boccaccini@fau.de

[c] Institute of Materials and Machine Mechanics, Slovak Academy of Sciences, 845 13 Bratislava, Slovakia

This journal is © The Royal Society of Chemistry 2024

J. Mater. Chem. B, 2024, **12**, 1875–1891 | 1875

(MBGs) are recognized biomaterials for bone regeneration due to their bioactivity, biocompatibility, and degradability.[7–9] Owing to their ordered mesoporous structure, large pore volume and high surface area, they are considered third-generation bioactive glass systems.[10] These characteristics enhance their capability to bond with bone tissue and restore the function of diseased, traumatized and damaged parts. MBGs are mostly synthesized as binary CaO–SiO_2 or tertiary CaO–P_2O_5–SiO_2 systems. The components (such as Ca, P and Si) in the MBG are directly involved in the bone regeneration process. Si helps in the calcification of bone tissues, whereas Ca and P (being the fundamental constituents of HAp) play a vital role in bone formation and resorption. Different therapeutic ions such as Sr, Mg, Zn, Ag, Cu, and Co can be added in the glass system individually as network modifiers (in critical concentrations) to enhance the biological properties (osteogenesis, angiogenesis, and biocide activity) of bioactive glasses.[11] Addition of Sr in a MBG scaffold, for example, stimulates osteogenesis *in vivo*. Co and Cu ions promote angiogenesis, while Zn and Ag ions provide antibacterial activity.[12,13] Among various therapeutic ions, Cu ions are frequently reported to induce angiogenesis and stimulate the development and maturation of blood vessels.[14] Moreover, Cu ions show antibacterial characteristics against *Bacillus subtilis* (*B. subtilis*), *Escherichia coli* (*E. coli*), and *Staphylococcus aureus* (*S. aureus*) by bonding with amine, imidazole, thiol, and carboxylic functional groups of microbial proteins.[15–17] Wu *et al.* synthesized Cu-doped $80SiO_2$–$5P_2O_5$–$15CaO$ MBG scaffolds (with up to 5 mol% of Cu) which were found to stimulate VEGF expression and HIF-1α in human bone marrow stromal cells (hBMSCs). The scaffold also encouraged gene expression related to bone formation (such as osteopontin, osteocalcin and alkaline phosphatase activity) that considerably enhanced the differentiation of hBMSCs into osteoblasts.[18] Romero-Sanchez *et al.* incorporated 5 mol% of Cu in the $80SiO_2$–$15CaO$–$5P_2O_5$ system. The result suggests that the *in vitro* cell culture study conducted on bovine aorta endothelial cells (BAECs) did not show toxicity. Instead, it promotes cell viability and its migration. The *in vivo* study performed on the *Danio rerio* zebrafish embryo assay revealed that ionic products obtained from Cu-MBG or MBGs significantly enhanced the angiogenesis activity.[19] Similarly, Mg ions played a vital role in bone metabolic activity by guiding new bone formation and directly interacting with integrin proteins to enhance cell adhesion and stability.[20,21] Shoaib *et al.* prepared Mg-doped MBG nanoparticles by the sol–gel method using F127 surfactant. The prepared Mg-MBG nanoparticles have the capability of serving two purposes: promoting bone regeneration and providing sustained delivery of the mitomycin C drug. The Mg-MBG exhibited biocompatibility and demonstrated lack of significant cytotoxic effects on normal human dermal fibroblast (NHDF) cells. When immersed in SBF, Mg-MBG formed HAp, further enhancing bioactivity. Additionally, at a pH of 6.4, Mg-MBG exhibited a high maximum cumulative drug release of 89%.[22] Various studies can be found reporting on doping glass systems with individual therapeutic ions.[23–31] While doping with single ions, either Cu or Mg, the MBG system might impart extra or tailored functionality to the biomaterial. For instance, Mg ions

can enhance osteoblastic activity, while Cu-doped MBG can induce angiogenesis and antibacterial properties. A small addition of co-dopant ions in the MBG composition might provide multiple functionalities to a single biomaterial. However, studies on co-doped systems are scarce. Kermani *et al.* prepared the Sr–Co-doped multicomponent MBG which imparted a positive effect on the osteoblast-like cell line (MG-63) and promoted pro-angiogenic capability with human umbilical vein endothelial cells (HUVECs).[32] Balasubramanian *et al.* specified that the co-substitution of Sr and Cu in the MBG system enhanced the angiogenic and antibacterial characteristics, and resulted in vascularized, functional bone tissue material for bone regeneration application.[33] Moghanian *et al.* developed sol–gel-based Cu/Mg substituted derivatives of 58S-BG with $60SiO_2$–$4P_2O_5$–$(31 - x)CaO$/$xMgO$–$5CuO$ composition (where $x = 0, 1, 3, 5, 8$, and 10) without using surfactants. The investigations concluded that up to 5 mol% MgO in BG resulted in the highest MC3T3-E1 preosteoblast cell proliferation, alkaline phosphatase activity, and antibacterial activity against *Staphylococcus aureus* bacteria.[34]

Referring to previous studies, this work aims to prepare a multipurpose Mg/Cu co-doped-MBG. According to the authors' best knowledge, such co-substitution of Mg and Cu in a silicate MBG system with $80SiO_2$–$15CaO$–$5P_2O_5$ composition has not been so far documented. The addition of therapeutic ions, such as Mg and Cu, in the MBG system holds significant potential for providing multiple functionalities. In particular, Cu can contribute to antibacterial and angiogenesis activities, while Mg can stimulate osteogenesis. In this research, a small amount of co-dopant ions, Cu and Mg (up to 4 mol%), with equal concentrations (in a 1:1 ratio) was added to the $80SiO_2$–$(15 - 2x)CaO$–$5P_2O_5$–$xMgO$–$xCuO$ mol% MBG system, where $x = 0, 0.5, 1$, and 2 mol%. This study tests the hypothesis that the co-substitution of Mg and Cu in the parent glass system can deliver enhanced biological features for bone tissue regeneration.

2. Experimental procedure

2.1 Mesoporous bioactive glass preparation

MBG with the composition $80SiO_2$–$5P_2O_5$–$(15 - 2x)CaO$–$xMgO$–$xCuO$ where $x = 0, 0.5, 1$, and 2 mol% was prepared using a sol–gel technique *via* the evaporation-induced self-assembly (EISA) method. The non-ionic Pluronic® P123 surfactant (Mn-5800, Sigma-Aldrich) was used as a structure-directing agent for MBGs. The preparation of MBG with $80SiO_2$–$5P_2O_5$–$14CaO$–$0.5MgO$–$0.5CuO$ composition was carried out by dissolving 4.2 g of the P123 surfactant in 63 g of ethanol (99.98%) with 1.05 g of 0.5 M HCl. Later, 7.56 g of tetraethyl orthosilicate (TEOS, ~98.0%, Merck), 0.82 g triethyl phosphate (TEP, ~99.8%, Sigma-Aldrich), and 1.50 g of calcium nitrate tetrahydrate ($Ca(NO_3)_2 \cdot 4H_2O$, 98–99%, VWR International GmbH), were added at 1 h intervals. The doping ion precursors, 0.0305 g of copper chloride ($CuCl_2$, 97%, Sigma-Aldrich) and 0.0583 g of magnesium nitrate hexahydrate ($Mg(NO_3)_2 \cdot 4H_2O$, 99%, Sigma-Aldrich) were added in 10 minute intervals and the solution was continuously stirred for 24 h at room temperature. Nearly

1876 | *J. Mater. Chem. B*, 2024, **12**, 1875–1891

This journal is © The Royal Society of Chemistry 2024

Table 1 Nominal compositions of prepared MBGs (in mol%)

Acronym	CaO	MgO	CuO	SiO_2	P_2O_5	Molar composition
80S	15	—	—	80	5	$80SiO_2$–$15CaO$–$5P_2O_5$
1MC	14	0.5	0.5	80	5	$80SiO_2$–$14CaO$–$5P_2O_5$–$0.5MgO$–$0.5CuO$
2MC	13	1	1	80	5	$80SiO_2$–$13CaO$–$5P_2O_5$–$1MgO$–$1CuO$
4MC	11	2	2	80	5	$80SiO_2$–$11CaO$–$5P_2O_5$–$2MgO$–$2CuO$

30 mL of the prepared sol was poured into a Petri dish of 100 mm diameter and placed inside a climatic chamber with ~75% of humidity and a temperature of 32–35 °C for 35 h to achieve gelation. After 35 h of incubation, the humidity control was turned off and the gels were aged for 7–9 days at the same temperature. Later, the dried gels were heated at 700 °C for 5 h to obtain co-doped MBG powders, which are thereafter termed as 1MC. The undoped MBG is denoted as control (basic) glass 80S. Table 1 displays the nominal compositions of the basic glass 80S and the co-doped MBGs, along with the corresponding doping percentages.

2.2 Characterization of MBGs

The calcination temperature of MBGs was determined using differential scanning calorimetry combined with thermogravimetric analysis, (DSC-TGA by PerkinElmer DSC 8500). The analysis was conducted in an ambient atmosphere, with the temperature ranging from 40 to 1000 °C while maintaining a heating rate of 10 K min^{-1}. The X-ray diffraction measurements were implemented within the 2θ range of 10–80° using a Miniflex 600 diffractometer with monochromatic Cu-Kα radiation. For the analysis, the diffractometer was utilized at a voltage of 40 kV and a current of 15 mA. For elemental analysis, scanning electron microscope JEOL JSM-IT500 equipped with an energy dispersive X-ray spectroscopy detector (SEM-EDX) was employed. Before the EDX analysis, the sample surface was coated with the carbon conductive layer. The chemical composition of the MBGs was verified *via* optical emission spectrometry with inductively coupled plasma (ICP-OES by Agilent 5100 SVDV, Mulgrave, Australia). To prepare the samples, 25 mg of MBG powder was dissolved in a solution consisting of 2 mL HNO$_3$ (conc. 67–69%, Analytika Ltd), 6 mL HCl (conc. 30%, Merck), and 0.5 mL HF (conc. 47%, VWR chemicals) at ambient temperature. The N$_2$ adsorption–desorption method (using a Belsorp-mini II analyzer, Microtrac, Japan) was carried out at a degassing temperature of 77 K to determine the surface area, pore volume and pore size distributions of MBGs. The development of ordered mesoporous structures in all MBGs was documented *via* transmission electron microscopy (TEM) using a 300 JEOL 1200EX system, (ThermoFisher Scientific Titan Themis) operating at the accelerating voltage of 200 kV.

2.3 *In vitro* bioreactivity

The capability of MBG powders to nurture a calcium phosphate (Ca-P) layer on its surfaces was evaluated under acellular *in vitro* conditions utilizing simulated body fluid (SBF) prepared by implementing Kokubo's protocol. Approximately 30 mg of each powder was immersed in a 20 mL of freshly prepared SBF, maintaining a pH of 7.4. The samples were then placed in a shaker incubator at 37 °C with 120 rpm for 4, 8, 24, 168 (7 day), and 336 h (14 days). Following each time interval, the supernatant was collected for pH measurement (pH per mV micro kit, FP20 benchtop, Ohio, USA) and an ion release study was performed using ICP-OES. The Ca–P layer development on the powders was evaluated by XRD, SEM and FTIR.

2.4 *In vitro* cytotoxicity

The cytotoxicity test was conducted using MG-63 cells, human osteoblast-like cells (obtained from ECACCS, Sigma-Aldrich, Germany) and NHDF cells, a normal human dermal fibroblasts cell line (obtained from ATCC PCS-201-010). All the cells were grown in Dulbecco's modified Eagle's medium (DMEM) obtained from Gibco, Germany and kept at 37 °C in an incubator with 95% air and 5% CO$_2$. The DMEM is prepared with the addition of 10 vol% of fetal bovine serum (FBS) obtained from Sigma-Aldrich, Germany and 1 vol% of penicillin–streptomycin (PS) from (Gibco, Germany). When MG-63 and NHDF cell lines reached their full confluency, they were seeded in a 24-well plate with a density of 1×10^5 cells per well along with the addition of 1 mL of DMEM to each well and incubated for 24 h.

In a parallel sample, MBGs were subjected to sterilization for 2 h at 160 °C. The MBG extract was prepared by placing 500 mg of sterilized powder to approximately 10 mL of DMEM (5 wt/vol%) and the mixture was incubated for 24 h. The extract was centrifuged at 4000 rpm for 15 minutes, passed through a 0.45 μm pore size filter, and then diluted to varying concentrations *i.e.*, 1 and 0.1 wt/vol% using DMEM. After 24 h of incubation, the cell medium was taken out, and 1 mL of the diluted extract of different concentrations (5, 1, and 0.1 wt/vol%) was added to the 24-well plates. The well plates were subsequently incubated for an additional 48 h. The MG-63 and NHDF cells only in cell media without the MBG extract were considered as the positive control (PC), while the cells treated with 6 vol/vol% dimethyl sulfoxide (DMSO) in DMEM were considered as the negative control (NC). All the experiments were completed in three replicates. The cell proliferation was examined using the WST-8 assay (by CCK-8, Sigma-Aldrich). After 48 h, the extract was removed, and 400 μL of a 1 vol/vol% WST-8 solution in DMEM was added to each well. The plates were then incubated for an additional 3 h, including blank samples that contained only the WST-8 solution in DMEM. Later, 100 μL of samples were added to 96 well plates to quantify the absorbance values using a microplate reader at 450 nm (PHOmo Elisa reader,

This journal is © The Royal Society of Chemistry 2024

J. Mater. Chem. B, 2024, **12**, 1875–1891 | **1877**

China). The cell proliferation percentage was evaluated using the equation:

$$\text{Cell viability (\%)} =$$
$$\frac{(\text{Absorbance of sample} - \text{Absorbance of blank})}{(\text{Absorbance of positive control} - \text{Absorbance of blank})} \times 100$$

Cell morphology was assessed by hematoxylin and eosin (H&E) staining. Hematoxylin has an affinity for the nuclei of the cells, changing the color to dark blue, whereas eosin binds with the extracellular matrix and cytoplasm of the cells and changes the color to red or pink. The staining was executed on the same 24-well plates using the WST-8 assay.

The leftover was discarded, washed with PBS (1 mL per well), and fixed with 4 vol/vol% of paraformaldehyde in PBS (conc. 400 μL per well) for 15 minutes. Later, the fixation solution was discarded, and the samples were washed with deionized water. 400 μL of concentrated hematoxylin was added to each well, and the plates were incubated for 15 minutes. Subsequently, the well plate was washed with deionized water, then with Scott's tap water (for 5 minute), and again with deionized water. Next, the cell plate was stained with eosin (conc. 400 μL mL^{-1}) for 5 minutes and later washed with 99.5% ethanol and dried at room temperature. After drying, the cell morphology was analyzed using an optical microscope (Primo vert, Carl Zeiss).

2.5 Antibacterial study

The antibacterial study of MBGs was performed using *S. aureus* (Gram-positive) and *E. coli* (Gram-negative) bacteria. The agar disk-diffusion method and turbidity methods were adopted to perform the antibacterial study of MBGs. Initially, the bacteria were grown in lysogeny broth (LB) medium for 24 h. For the agar method, MBG pellets with thicknesses of ~ 2 mm and ~ 14 mm diameter were produced employing a hydraulic press (by PE-010, Mauthe Maschinenbau) applying a 50 MPa pressure to ~ 200 mg of powder. Afterward, the pellets were sterilized by heating them to the temperature of 160 °C for 2 h. The optical density of the bacterial suspension was analyzed employing a visible light spectrophotometer at 600 nm and an initial set up at 0.015 (*i.e.* $\sim 1 \times 10^7$ colony forming units per mL). Then, approximately 20 mL of LB agar media was transferred to Petri plates while hot. Once the agar media hardened, 20 μL bacterial suspension was spread evenly on the agar surface. MBG pellets were then positioned in the central region of the agar media and incubated overnight. The next day, the zone of inhibition encircling the pellets and free of the bacteria was estimated using a ruler scale from digital images.

For the turbidity study, MBG extract concentrations of 5 wt/vol% (conc. 50 mg mL^{-1}) and 1 wt/vol% (conc. 10 mg mL^{-1}) were prepared using LB media and placed in an incubator for 24 h at 37 °C with a continuous shaking speed of 120 rpm. MBG powders were filtered out and the supernatant was collected for the test. Then, 20 μL of each bacteria suspension was mixed with 2 mL of the extract and incubated for 24 h. The relative

S. aureus and *E. coli* bacterial viability was calculated using the equation:

$$\text{Bacterial viability (\%)} = \frac{\text{optical density of sample}}{\text{optical density of control}} \times 100$$

2.6 Statistical analysis

Statistical analysis was conducted employing one-way variance ANOVA followed by the Tukey test. All the tests were executed using OriginLab 2018 software. Quantitative results are displayed as the mean ± standard deviation. The probability (P) value with a significance level of $P < 0.05$ was calculated to facilitate a multiple comparison.

3. Results and discussion

3.1 Thermal, physicochemical, and textural characterization of MBG

The DSC-TGA thermograms of the as-prepared MBG powder were recorded to estimate suitable calcination temperatures. Fig. 1 presents the DSC-TGA plot of the basic, undoped, 80S glass and the glass with the highest content of co-dopants: 4MC (containing up to 4 mol% co-dopant ions *i.e.*, 2 mol% MgO and 2 mol% CuO). The 80S glass showed a faster mass loss of $\sim 67.32\%$ in total, compared to 4MC with a $\sim 68.90\%$ mass loss when heated up to 1000 °C. Due to the small ionic radius of Cu and Mg ions, (0.72 Å and 0.65 Å, respectively) compared to Ca (1.06 Å), the addition of dopants may contribute to the formation of a glass with a more compact (denser) structure.

The observed weight loss is attributed to the preparation method, *i.e.* the sol–gel conjugated EISA technique, which was executed in a closed chamber by maintaining a humidity of ($\sim 75\%$) and a temperature of 32 ± 3 °C. During the process, the molecular precursor (the metal alkoxide) dissolves in a water-alcohol solution and transforms to gel through hydrolysis and condensation reactions. The obtained MBG gel is wet, containing a significant amount of water. The pluronic surfactant controls mesoporous texture inside the sol–gel glass. The decomposition of organic moieties present in sol–gel glass is responsible for the additional mass loss. The major change of mass loss in 80S glass was observed in two steps (Fig. 1(a)). The 1st step from 40 to 190 °C ($\sim 6.94\%$ mass loss) was due to the elimination of adsorbed surface water. The subsequent major mass loss noted from 190 to 503 °C (up to $\sim 60\%$) with two exothermic events at 202 °C and 317 °C was attributed to the vaporization of volatile compounds and decomposition of surfactant molecules, respectively. An endothermic asymmetric peak at 462 °C refers to the decomposition of nitrates.[35,36] In the DSC-TGA record of the co-doped 4MC glass (Fig. 1(b)), a mass loss ($\sim 12.75\%$) in the temperature interval from 40 to 221 °C accompanied by two exothermic peaks at 82 °C and 194 °C was determined and attributed to the removal of adsorbed water molecules. Decomposition reactions of organic (surfactant) and inorganic molecules (nitrates and chlorides) were detected in the range from 221 to 462 °C with a mass loss

1878 | *J. Mater. Chem. B*, 2024, **12**, 1875–1891

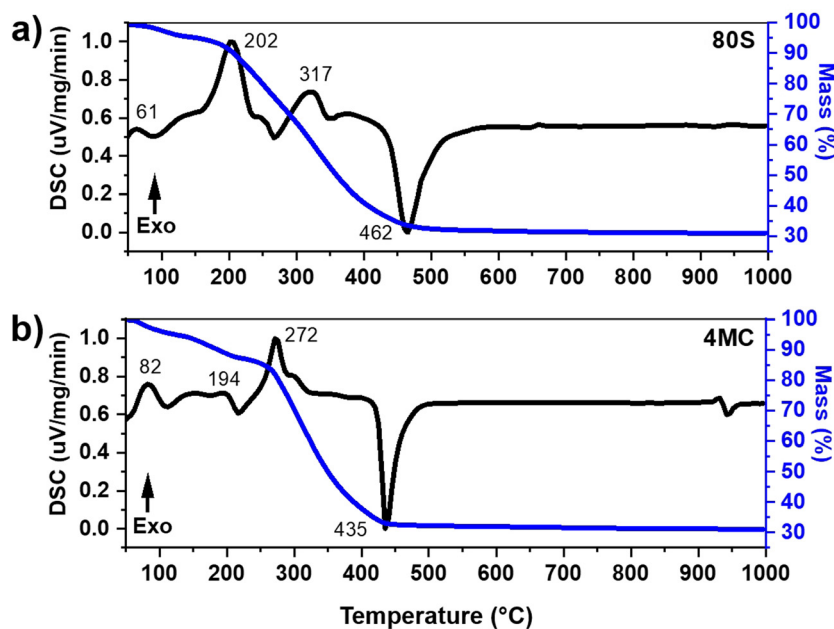This journal is © The Royal Society of Chemistry 2024

Fig. 1 DSC-TGA plot of (a) basic glass 80S and (b) co-doped 4MC powders.

of $\sim$55%. A shift of an endothermic peak towards higher temperatures was observed for 80S glass at 462 °C possibly because of the presence of a significant amount of calcium nitrate precursor in comparison to Mg–Cu co-doped MBG (4MC) which showed an endothermic peak at 435 °C. A similar pattern of the endothermic peak shift was observed by Kermani et al.[32] The DSC-TGA plot indicates that all organic precursors and surfactant agents were lost around 650 °C. Based on the DSC records, all the as-prepared co-doped MBGs were calcined at 700 °C for 5 h at a heating rate of 2 °C min^{-1}.

Table 2 summarizes the resultant chemical composition of the MBG system after calcination, as determined by ICP-OES. The prepared MBG glass contains a large amount of SiO_2 i.e., up to 80 mol%: Si is lost during combustion/decomposition because of the reaction with HF and the formation of volatile silicon tetrafluoride. Therefore, the amount of SiO_2 is obtained by subtracting the sum of the contents of other oxides from 100%. The contents of dopant oxides (MgO and CuO) were found to correspond to their respective nominal amount in the resultant MBG glass. The lower amount of P_2O_5 compared to its nominal content observed for all MBGs was attributed to transformation from a solid to liquid state during the phase transition in the course of calcination, resulting in the evaporation of P_2O_5 from the system.[37] Moreover, the lower amount of P_2O_5 in all MBG systems could be also partially explained by the different hydrolysis rates of

TEOS and TEP precursors that cause rapid condensation of SiO_2 particles lacking P ions.[38,39]

Fig. 2 shows the XRD patterns of basic 80S and co-doped MC-MBG powders. The presence of wide diffusion halos in the 2θ range from 15 to 35° without any sharp diffraction maxima refers to the amorphous nature of all prepared glass compositions.[40]

Elemental analysis of the MBGs was carried out via SEM-EDX. The elemental maps and spectra for all co-doped MBGs are shown in Fig. 3(a). Lateral homogeneous distribution and presence of all scanned elements (Si, Ca, P, Mg, Cu) were determined, and contaminant residues were not detected on the analysed powders (Fig. 3b).

The nitrogen (N_2) adsorption–desorption study was performed to determine the shape of the isotherms, pore structures and surface areas of prepared MBG powders. All systems showed Type IV adsorption–desorption isotherms (Fig. 4). For all measured MBGs samples, the adsorption–desorption curves in the (P/P_0) range from 0 to 0.4 overlap, indicating the absence of microporosity. At (P/P_0) from 0.4 to 0.7, the curves are vertical and parallel to each other, corresponding to the H1 hysteresis type. This distinct hysteresis loop indicates the creation of uniform cylindrical mesopores, which are open on both ends.[41] Table 3 provides detailed information about surface areas, pore sizes and total pore volumes of all prepared powders. All co-doped powders were characterized by a high

Table 2 Chemical compositions of MBG powders calculated from data obtained using the ICP-OES method together with standard deviations obtained from three parallel measurements

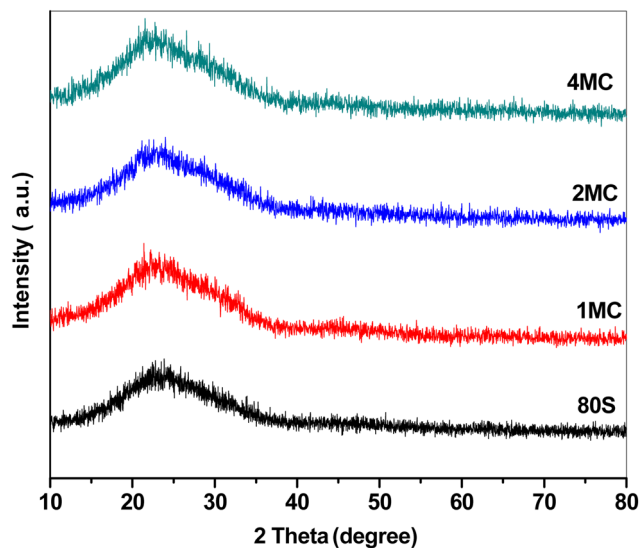| Acronym	CaO (mol%)	MgO (mol%)	CuO (mol%)	SiO_2 (mol%)	P_2O_5 (mol%)
80S	14.8 ± 0.4	—	—	84.9 ± 0.4	<0.5
1MC	15.2 ± 0.1	0.52 ± 0.02	0.544 ± 0.002	83.3 ± 0.4	<0.5
2MC	13.2 ± 0.2	1.001 ± 0.005	1.04 ± 0.01	84.57 ± 0.06	<0.5
4MC	11.91 ± 0.09	2.143 ± 0.006	2.13 ± 0.01	83.3 ± 0.1	<0.5

This journal is © The Royal Society of Chemistry 2024

J. Mater. Chem. B, 2024, **12**, 1875–1891 | **1879**

Fig. 2 XRD graph of the basic glass and the Cu, Mg co-doped mesoporous powders.

specific surface area of up to 320 m^2 g^{-1}, which was higher than that of the basic glass 80S (253 m^2 g^{-1}). The increased concentration of bivalent ion dopants disturbed the self-organization of surfactant moieties resulting in fewer surfactant molecules involved in creating each template.[42] This results in the formation of a higher number of smaller template sites. Later, after calcination, the smaller template sites transform into higher number of pores with smaller pore sizes, thus increasing the specific surface area of the material.

The development of a uniform cylindrical mesoporous structure was further examined *via* TEM. All MBG powders showed fringes that appear as parallel lines, representing the formation of ordered mesoporous textures. The addition of co-dopants Mg and Cu did not disrupt the pattern of mesoporosity. The use of the non-ionic pluronic surfactant and the condensation of inorganic components through the EISA process with controlled humidity (~75%) and a temperature of 32–35 °C affect the development of organized mesostructures.[42] Formation of strong hydrogen bonds between the protonated EO (ethylene oxide) of the pluronic surfactant and the silica oligomers promotes the formation of an organized silicatropic liquid crystal phase and the creation of an ordered mesoporous structure (Fig. 5).[43]

3.2 Acellular *in vitro* bioactivity study

The release of Ca, P, Si, Cu, and Mg ions and the pH change were examined to understand the chemical reactions of MBG in contact with SBF *in vitro* (Fig. 6). The concentrations of elements (Ca and Mg) already present in SBF were subtracted from the measured values. A series of chemical reactions, *i.e.*, leaching of ions, dissolution, and precipitation, occur during the interaction of the glass with the SBF solution resulting in HAp layer deposition on the glass surface and later, under *in vivo* conditions, formation of a bond with living bone tissues. The dissolution of a silicate glass network in contact with the SBF solution through an attack of hydroxyl ions followed by

breaking Si–O–Si bonds was detected by increased silicon concentration with time. Dissolution of silicate glasses in aqueous media depends on the amount of silica present in the glass system.[44,45] It was assumed that the high amount of silica in studied mesoporous glasses positively affects the rigidity of the glass network by the development of more bridging oxygen bonds. Dopant ions incorporated into the structure in lower amounts could be then released into a body fluid in a more controlled way. Varying the amount of glass modifiers (Cu, Ca, Mg) destabilizes the glass structure and causes lower chemical stability in the aqueous environment compared to quartz glass.[46] In the present MBG system, the amount of SiO$_2$ was kept constant (up to 80 mol%), and doping oxides (CuO–MgO) were added to substitute CaO in the glass network. Apart from the chemical composition, the textural properties and specific surface area in contact with the leaching solution influence the durability of glass and release of the therapeutic ions. Reactivity of the 85SiO$_2$–10CaO–5P$_2$O$_5$ mesoporous glass is assumed to be high.[41] Despite this fact, testing procedures for ion release from the MBGs powders follow the standard procedure reported in the literature with the sampling intervals of 1 to 3 days,[47] when the saturation concentration of leached ions is achieved. In concentration–time dependence plot, the achievement of the equilibrium state is shown as a plateau. When the equilibrium is exceeded, precipitation starts, resulting in the depletion of some ions from the solution. A time interval for sampling was also designed to monitor the release in the first 8 h of exposure to detect the concentration of dissolved ions before the equilibrium between glass and solution is achieved. Higher concentrations of Si and Ca were measured in SBF media for the initial time after soaking of all co-doped MBG, documenting low chemical durability of the glass. Lower amounts of Si and Ca leached from the basic glass (80S) into SBF were detected possibly due to the lower specific surface area (253 m^2 g^{-1}) in comparison to all co-doped MBG glasses (300–320 m^2 g^{-1}). A sudden decrease of Ca and P content after the first day signals the precipitation of an apatite phase from the solution, which was already supersaturated with respect to HAp formation. The cationic exchange with H$_3$O$^+$ ions usually leads to enhanced hydroxyl ions' concentrations in SBF documented by the increase of pH values (>7.4) at the temperature of ~32 °C.[48,49] Unlike for the basic 80S glass, the release of Mg in line with Ca from co-doped MBG into the SBF solution contributed to the increase of the solution pH (as shown in Fig. 6), contributing to the faster dissolution of the Si–O–Si network.

Overall, steady leaching of Mg and Cu was observed for the MBG with a dopant concentration of up to 2 mol%. According to Huang *et al.*, a slow release of Cu with a concentration <1 mg L^{-1} improved the angiogenesis and osteogenesis activity of Cu-doped nanocomposite coatings on the titanium substrate.[50] However, Kong *et al.* concluded that the optimal range of Cu concentration for the expression and stimulation of VEGF was between 14 and 57 mg L^{-1}.[51] Moreover, a higher release of Cu ions up to 36.2 mg L^{-1} following 1 day of soaking in SBF was reported to be non-toxic for bone marrow-derived stem

1880 | *J. Mater. Chem. B*, 2024, **12**, 1875–1891

This journal is © The Royal Society of Chemistry 2024

Fig. 3   Lateral SEM-EDX mapping of co-doped mesoporous glass powders (a); EDX spectra (b) measured during mapping.

cells.[52] In the present study, Cu and Mg were co-doped in an equal concentration of up to 4 mol%. The highest release of Cu was measured from the 4MC system (< 32 mg L^{-1} after 7 days). Hypothetically, the release of ions from all co-doped systems could improve angiogenesis while being non-toxic for the cells.

The acellular bioreactivity of glass mostly relies on surface reactions that gradually enhanced with the CaO/MgO ratio.[53] A fast release of Mg ions observed later up to 7 days becomes more stable with time, especially for MBG doped with 0.5 to 1 mol% of magnesium (1MC, 2MC). From the sample 4MC, Mg was gradually leached for 14 days. Dietrich et al. stated that the incorporation of Mg significantly influenced the glass dissolution by disrupting the Si network. However, reduced crystallization of the HAp layer on bioactive glass surfaces was reported in the presence of Mg.[54]

The results of the FTIR (Fig. 7), XRD (Fig. 8), and SEM (Fig. 9) analyses show that all co-doped MBGs might be bioactive if expressed in terms of their capability to develop an apatite phase.

The development of a new Ca–P phase onto the surface of co-doped powders was studied by measuring FTIR spectra and focusing on P–O bands at 560 and 602 cm^{-1} in the spectra of the samples immersed in SBF from 4 h to 14 days (Fig. 7). A common band of silica was observed for all MBGs at around 1040 and 440 cm^{-1} which related to the asymmetric bending vibration of Si–O–Si and symmetric stretch of Si–O bands at 800 cm^{-1}. After 4 h of soaking, only silica bands were observed for all MBGs. With an increasing soaking time of MBGs in SBF, new P–O bands were detected at 560 cm^{-1} that indicated the development of an amorphous phosphate phase. The basic glass 80S and 1MC showed a faster formation of the phosphate

This journal is © The Royal Society of Chemistry 2024

J. Mater. Chem. B, 2024, 12, 1875–1891 | 1881

Fig. 4 Nitrogen adsorption/desorption isotherm of basic glass (80S) and Cu–Mg doped MBGs.

Table 3 Textural properties of the basic glass (80S) in comparison to Cu–Mg doped MBGs

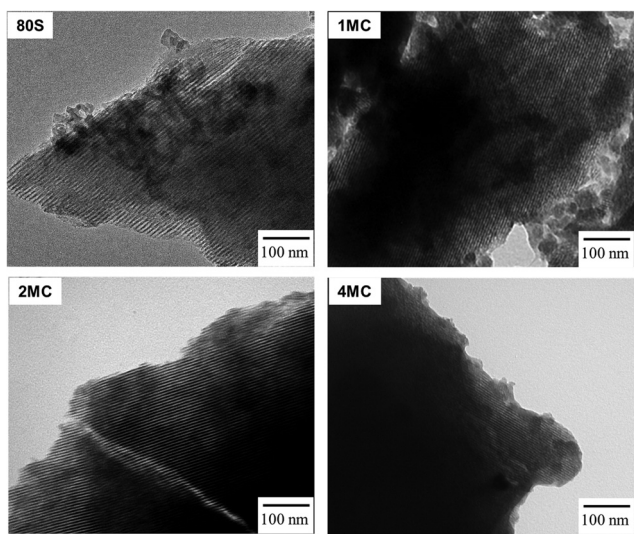| Acronyms	Surface area ($m^2\ g^{-1}$)	Pore size (nm)	Pore volume ($cm^3\ g^{-1}$)
80S	253	5.20	0.329
1MC	310	5.20	0.177
2MC	320	5.13	0.202
4MC	304	5.11	0.182

Fig. 5 TEM images of basic glass (80S) and Cu-Mg doped MBG powders.

phase compared to other co-doped glasses, showing the presence of the P–O bands only after 8 h of soaking. 2MC and 4MC co-doped glasses showed the formation of the P–O bands after 1 day of SBF soaking. With increasing soaking time, the band at 560 cm^{-1} split into two distinguished bands at 560 and 602 cm^{-1} that indicated the formation of a crystalline phosphate phase. For the 80S and 1MC glass, P–O bands formed only after

1 day of soaking belong to the crystalline phase, while 2MC and 4MC showed such bands only after 7 days of SBF immersion.

To verify the development of a new crystalline calcium phosphate phase, XRD analysis was carried out after 1, 7, and 14 days of contact of the samples with the SBF solution (Fig. 8). Diffraction maxima were observed in the range of $(20°–80°)\ 2\theta$. A diffraction maximum at $2\theta = 32.2°$ was detected only after 1 day of SBF soaking for the glasses 80S and 1MC. The 2MC and 4MC samples showed a slight delay in the formation of diffraction maximum at $32.2°$ observed only after 7 days of SBF soaking (Fig. 8(b)). Overall, all the powders showed a typical diffraction pattern with the diffraction maxima at 2θ angles $26.1°$, $32.2°$ and $49.7°$ that are commonly attributed to the HAp phase (JCPDS no. 01-086-0740), indicating the development of an apatite layer on both undoped and Cu and Mg co-doped MBG powders following 14 days of soaking in the SBF solution.[55]

Further examination of the MBG surfaces *via* FESEM (Fig. 9) following 14 days of exposure in SBF showed the occurrence of a HAp layer with a flake-like microstructure. In previously published works, samples with such a microstructure were labeled as *in vitro* bioactive.[56,57] Co-doping with Cu and Mg ions did not visibly affect the microstructure of the phase(s) detected on the surface.

3.3 *In vitro* cytotoxicity study

The results of the MG-63 and NHDF cell viability tests in contact with varying concentrations of MBG extracts are shown in Fig. 10. The test was based on the release of Ca, P, Si, Cu, and Mg ions from the MBGs for 24 h in DMEM at 37 °C. When the MG-63 cells were being cultured with the 5 wt/vol% extract, the viability was > 50% for co-doped MBG and > 80% for 80S glass (Fig. 10(a)). For lower concentrations (1 and 0.1 wt/vol%), no significant difference for MG-63 cell viability was observed and was higher/or equal to 90% for both co-doped and basic 80S MBGs.

However, when MBG extracts were cultured with NHDF cell lines, the cell viability was lower than for the MG-63 cell lines. The viability of NHDF cells cultured with varying concentration of MBG extracts following 48 h of incubation is presented in Fig. 10(b). The cells in contact with the 5 wt/vol% extract showed the toxicity effect of the extract, and the viability was below 50% for all co-doped MBG systems. The NHDF cells in contact with 1 wt/vol% of the extract achieved viability > 60% for the co-doped MBG systems and ∼ 90% for the basic 80S glass. For the lowest concentration (0.1 wt/vol%), the cell viability was above 80% for the co-doped MBGs and around 95% for the 80S glass. Overall, for each cell line, the viability of cells was found to increase with increased dilution. The lowest cell viability for each MBG extract concentration (5, 1, and 0.1 wt/vol%) was reported for the MBG system doped with the highest amount of Cu (4MC). For 24 h, copper ions are released from the 4MC sample in cell medium in higher amounts compared to MBG with CuO content ≤ 1 mol%. The pH increase because of the release of greater amounts of Mg and Ca could also negatively influence cell viability. Several published works conveyed that the release of therapeutic ions in
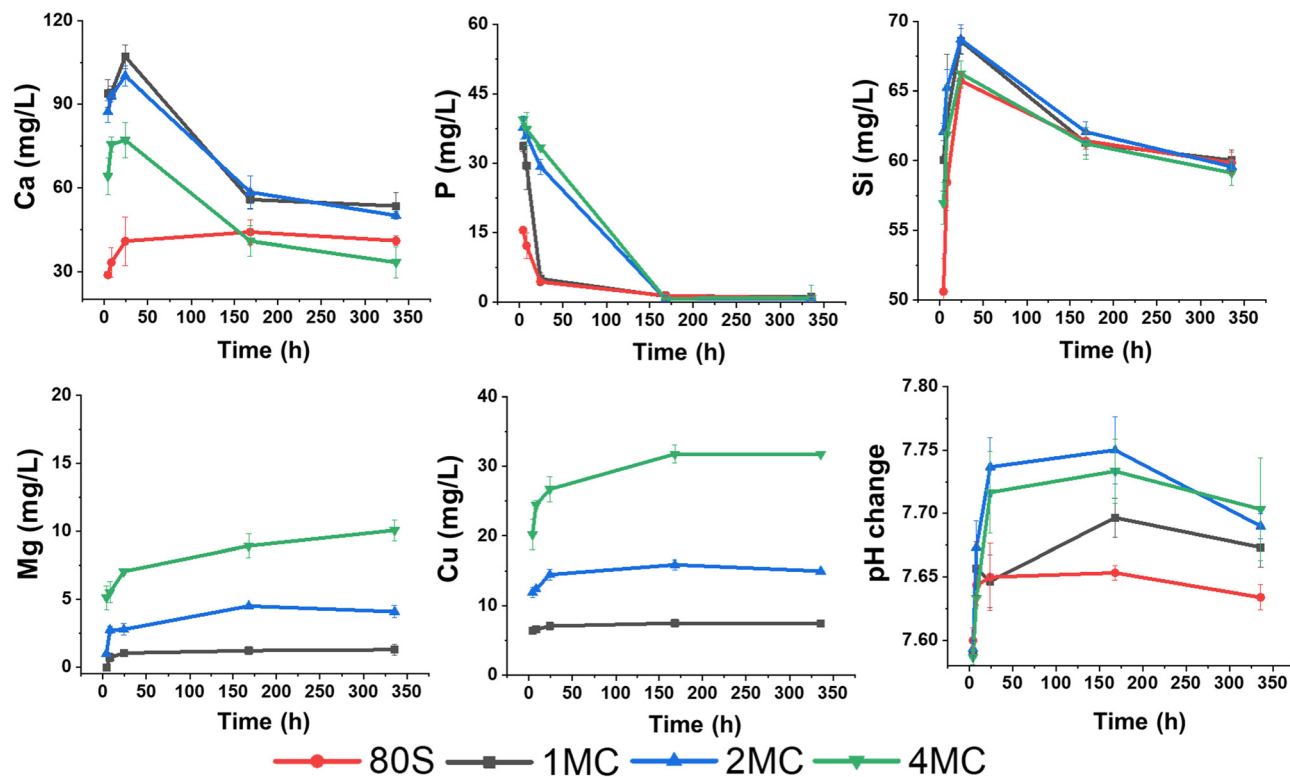
1882 | *J. Mater. Chem. B*, 2024, **12**, 1875–1891

This journal is © The Royal Society of Chemistry 2024

Fig. 6 Release profiles of Ca, P, Si, Cu, and Mg (mg L^{-1}) from the 80S, 1MC, 2MC, and 4MC MBGs in SBF medium and changes in the pH value after 4 h, 8 h, 1 day, 7 days and 14 days.

Fig. 7 FTIR spectra of MBGs between 1600 and 400 cm^{-1} after placing them in SBF from 4 h to 14 days.

high concentration can be toxic for the cells, resulting in a lower cell viability in co-doped MBG systems in comparison to undoped MBGs.[58] The undoped 80S MBG containing only Si, Ca, and P ions showed viability close to 100%.

In the cytotoxicity study, 1×10^5 cells were placed on each well of the plates with 1 mL of an extract with different concentrations. The 1 wt/vol% MBG extract contained 10 mg mL^{-1} of MBG powder which was too high for the cells to grow and proliferate. The 1 wt/vol% MBG extract showed higher

cell viability for the MG-63 cells (above 80%) than for the NHDF cells with cell viability >60%. The MG-63 cell lines are osteoblast-like cells commonly used as osteoblast models to examine bone cell viability. However, they are osteosarcoma-derived cells whose molecular composition such as extracellular matrix is not well defined.[59] The MG-63 cell lines possess a characteristic where they inherently lack control over their cell cycle resulting in continuous and infinite proliferation capability.[60] Thus, during differentiation, MG-63 cells tend to divide rapidly and grow faster

This journal is © The Royal Society of Chemistry 2024

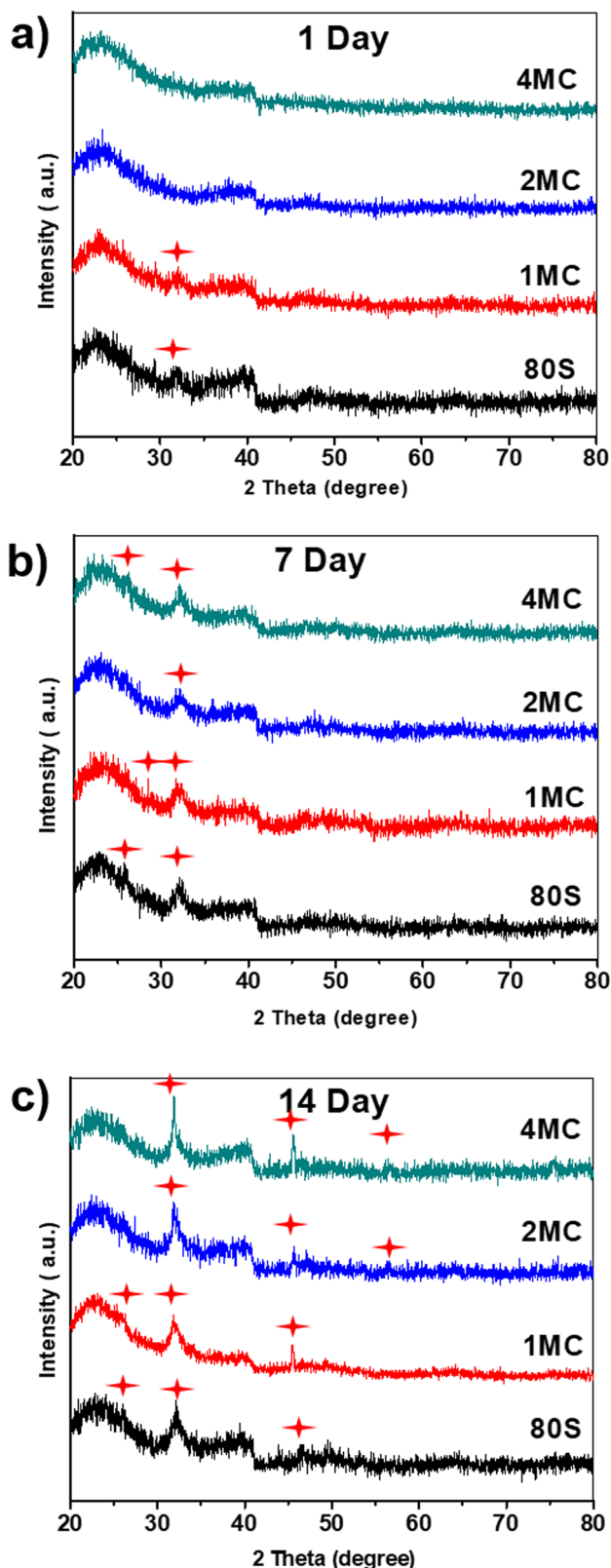*J. Mater. Chem. B*, 2024, **12**, 1875–1891 | **1883**

Fig. 8 XRD patterns of the investigated MBGs after placing them in SBF for (a) 1 day, (b) 7 days, and (c) 14 days; (formation of new hydroxyapatite phase marked by red stars).
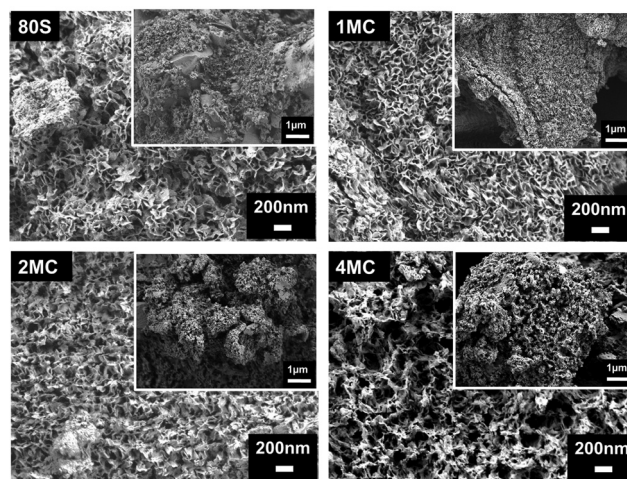

Fig. 9 FESEM image of the MBGs surface after placing in SBF for 14 days. The inset shows the same microstructure at a lower magnification.

representing immature phenotype while normal cells like NHDF cells undergo a process of maturation and then performed their specialized functions. This may be the reason for the higher cell viability percent of the MG-63 cell line in comparison to NHDF cells. Nevertheless, if the cell viability is above 60%, then all co-doped MBG samples can be considered non-toxic. The incorporation of co-dopants in the MBG structure, up to a concentration of 2 mol% (2MC) can be thus considered to be favorable for cell proliferation and viability.

The light microscopy images of H&E stained MG-63 and NHDF cells cultured with 1 wt/vol% of MBG extracts are shown in Fig. 11. Fig. 11a implies that the MG-63 cells adhered, grew, and spread all over the glass surfaces. The cell morphology ranged from oval to spindle-like for all the samples including the positive control.

When the NHDF cells were cultured with 1 wt/vol% extract, the cell morphology was elongated with thin flat, or wavy nuclei, which is a typical morphology of fibroblast cells (Fig. 11b). However, microscopy images confirmed that the MG-63 osteosarcoma cell lines are significantly smaller in size when compared to NHDF cells.

All the cells showed a spindle-shaped morphology and they were joined and scattered when they proliferated over the surfaces. A homogeneous monolayer of cells was observed for all samples cultured with NHDF cells. The cells in the NC appeared as individual cells or as clusters of cells. The incorporation of co-substituted (Mg and Cu) ions (up to 4 mol%) did not change the morphology of cells when compared to PC and 80S for both MG-63 and NHDF cell lines. Overall, microscopy examination confirmed that the confluence of MG-63 and NHDF cells with 1 wt/vol% extract is in line with the WST-cell viability results.

3.4 *In vitro* antibacterial study

Antibacterial study of MBGs was performed using *E. coli* and *S. aureus* bacteria. The study was performed using two techniques, the agar disk-diffusion method (using solid agar media) and the turbidity method (using Luria Broth media).

1884 | *J. Mater. Chem. B*, 2024, **12**, 1875–1891

This journal is © The Royal Society of Chemistry 2024

Fig. 10 Relative cell viability of (a) MG-63 cells and (b) NHDF cells cultured with varying concentrations (0.1, 1, and 5 wt/vol% MBGs extract) with the positive control (PC) and negative control (NC), $n = 9$, samples studied in three replicates, (*$p < 0.05$).

Fig. 11 H&E-stained microscopy pictures of MG-63 cells (a) and NHDF cells (b) cultured with 1 wt/vol% extract of MBGs.

For the disk diffusion method, sterilized MBG pellets were positioned on solid agar media with bacteria and incubated at 37 °C overnight. Fig. 12 shows the photographs of MBG pellets (80S, 1MC, 2MC, and 4MC) together with control discs with *E. coli* (G−) and *S. aureus* (G+) bacteria. As per the SNV 195920-

1992 standard protocol, a system can be classified as antibacterial if it can form an inhibition zone >1 mm.[61] The incorporation of Cu in the present system was expected to induce antimicrobial properties as additional functionality to the MBGs. The basic glass 80S did not show any inhibitory effect

This journal is © The Royal Society of Chemistry 2024

J. Mater. Chem. B, 2024, **12**, 1875–1891 | **1885**

Fig. 12 Photographs of MBG pellets with the zone of inhibition, cultured with *E. coli* (G−) and *S. aureus* (G+) bacteria using agar disk diffusion techniques.

while co-doped MBG pellets formed zones of inhibition. With the progressive increase in the Cu content, the zone of inhibition was more noticeable. The zone of inhibition was larger for MBGs with a higher concentration of dopants: 4MC pellets showed the size of the inhibition zone for *E. coli* $\sim$3.6 mm, while the size of the 2MC inhibition zone was $\sim$2.5 mm, which decreased to $\sim$1.5 mm for 1MC. The zone of inhibition for *S. aureus* was slightly larger. For 4MC, the inhibition zone was of $\sim$3.8 mm, while 2MC and 1MC showed the size of the inhibition zone of $\sim$2.7 mm and $\sim$2 mm, respectively. Various factors possibly contributed to the antibacterial characteristics of the bioactive glasses such as the release of Ca and Cu ions in bacteria medium which might cause disturbance in the membrane potential of bacteria and creates an osmotic pressure. The bacterial cell wall has a negative electrical charge due to the presence of carboxylic groups in its lipoproteins.[62] The Cu ions released from MBG are electrostatically attracted to bacteria, potentially damaging the cell wall, creating enzyme dysfunction, and leading eventually to bacterial death.[63] The test was carried out using solid agar media of a lower capacity for the diffusion of ions. The release of ions from pellets in liquid broth medium is therefore different from the solid agar.

For the turbidity method, two concentrations, 5 and 1 wt/vol% of MBG powders in LB medium, were preferred to estimate the viability of bacteria cells and the inhibitory effect of MBG extracts. Before the addition of bacterial strains into the MBG extract, pH measurements were performed to understand the consequence of pH change on antibacterial activity. The pH value of the LB medium used as a control was 7.0, which is an ideal value for the growth of bacteria.[64] However, the pH value of the MBG extract increased after 24 h of incubation and

Fig. 13 pH measurement of 1 and 5 wt/vol% MBG extract concentrations in LB media after 1 day of incubation.

ranged from 7.5 to 8.5 (Fig. 13). The rise in the pH value was the result of the release of high amounts of bivalent cations (Ca, Mg) into the extract. It is assumed that a shift of the pH value towards alkaline values is possibly stressful for bacteria, which in response changes the morphology and modifies the expression of proteins and genes of bacteria.[65]

The results of extracts with the concentration of 5 and 1 wt/vol% cultured with bacterial strains and incubated for 24 h at 37 °C to study the inhibitory effect of MBGs are presented in Fig. 14. The bacteria cultured only in Luria Broth

1886 | *J. Mater. Chem. B*, 2024, **12**, 1875–1891

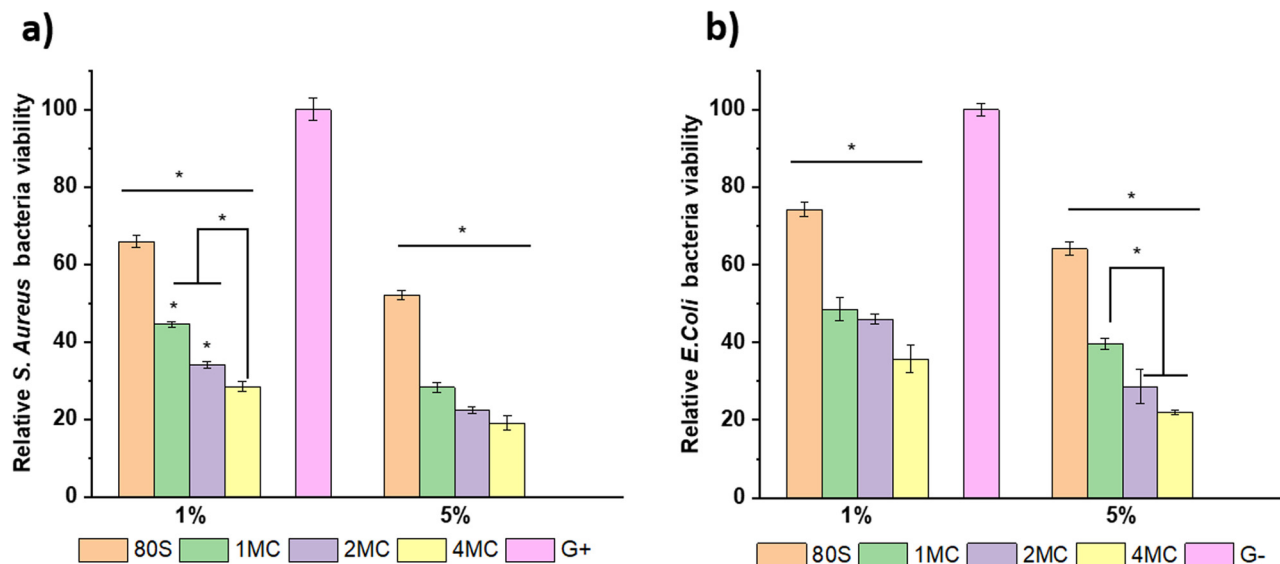This journal is © The Royal Society of Chemistry 2024

Fig. 14 Relative bacterial viability of Gram-positive *S. aureus* (a) and Gram-negative *E. coli* strains (b), cultured with 1 and 5 wt/vol% extracts of MBGs ($n = 9$, G+ = *S. aureus*, G− = *E. coli*, samples in triplicate, *$p < 0.05$).

medium are considered as control (C) and are normalized as 100%. A stronger inhibitory effect was observed for *S. aureus* in comparison to *E. coli* for all MBG extract concentrations, corroborating the result obtained from solid agar media tests. The basic glass 80S showed *S. aureus* bacterial viability around $\sim 52\%$ for 5 wt/vol% extract and $\sim 65\%$ for 1 wt/vol% extract. When 80S was cultured with *E. coli*, the viability of the cell was slightly higher, *i.e.*, $\sim 64\%$ for 5 wt/vol% and $\sim 74\%$ for 1 wt/vol% extract. For co-doped glasses, the inhibitory effect was more evident with the sequential increment in the concentration of co-doped ions for both bacterial strains. The 5 wt/vol% extract from co-doped MBGs showed a significantly higher inhibition effect for both bacterial strains and the viability was reduced to <50%. It is noted that the 5 wt/vol% concentration extract was highly toxic for both bacterial strains, although it was also cytotoxic for NHDF cell lines. It is important to examine a particular concentration at which MBGs still show cytocompatibility but also have the potential to restrict the growth of bacteria. For 1 wt/vol% concentration, the 4MC glass was more effective against *S. aureus*, with the viability of around $\sim 28\%$, which was lower in comparison to 2MC ($\sim 34\%$) and 1MC ($\sim 44\%$). For *E. coli*, the 4MC glass showed a relatively lower inhibitory effect. The bacteria viability was $\sim 35\%$ for 4MC, 46% for 2MC, and 48% for 1MC. In general, the concentration of solute molecules within the cytoplasm of bacteria exceeds that of its surrounding environment resulting in positive pressure in the bacteria cell membrane.[66] So, when MBG extracts come into contact with bacteria, a rapid rise in the concentration of external solutes creates rapid water efflux and a reduction in the pressure on the cell membrane.[67,68] As a result, alteration in bacterial cell volume, size, shape, and cell membrane stress levels occurs. Thus, the morphological changes lead to bacteria mortality. Copper ions produce reactive oxygen species (ROS) through the partial reduction of O_2, leading to the generation of hydroxyl radicals ($\bullet OH$).[69] These radicals exhibit high reactivity and have the potential to harm or disrupt the integrity of bacterial cells. ROS engage in direct interactions with DNA, lipids, and protein molecules, thereby contributing to oxidative stress.[70]

4. Conclusions

The sol–gel-based EISA technique was employed to prepare MBG 80S and Mg-Cu doped MBG powders with $80SiO_2$–$5P_2O_5$–$(15 - 2x)CaO$–$xMgO$–$xCuO$ glass composition where $x = 0, 0.5, 1$ and 2 mol%. BET results indicated that all powders were characterized by a cylindrical mesoporous texture and a large surface area of up to 320 m^2 g^{-1}. *In vitro* acellular bioreactivity of all prepared MBGs was documented by the creation of the Ca–P phase after soaking in SBF for 14 days. Cytotoxicity tests showed a noteworthy difference between the viability of MG-63 and NHDF cell lines. The MBG extract with 1 wt/vol% concentration showed high viability of MG-63 cells ($\sim 90\%$), while NHDF cells showed comparatively lower viability ($\sim 60\%$). Conversely, the co-doping of up to 2 mol% in MBGs showed NHDF cells' viability >75%. Antibacterial tests using the disk diffusion method revealed that an increased amount of dopants in MBGs expands the zone of inhibition. Similarly, the turbidity test performed using a 1 wt/vol% extract of MBGs with 4 mol% of co-dopants exhibited the highest inhibitory effect on bacteria. The basic 80S MBG did not form a zone of inhibition for bacteria in a solid agar medium. Employing Mg and Cu (up to 2 mol%) in the MBG system might play a central role in stimulating new tissue formation by Cu and Mg ion delivery within the bone regeneration process. The novel Mg and Cu co-doped MBGs can be promising multi-functional candidates as bioactive fillers with antibacterial properties.

This journal is © The Royal Society of Chemistry 2024

J. Mater. Chem. B, 2024, **12**, 1875–1891 | **1887**

Author contributions

Akrity Anand: conceptualization, methodology, validation, investigation, data curation, visualization, and writing – original draft. Hana Kaňková: formal analysis and validation. Zuzana Hájovská: TEM analysis. Dušan Galusek: validation, writing – review & editing, and funding acquisition. Aldo R. Boccaccini: conceptualization, validation, supervision, writing – review & editing, and funding acquisition. Dagmar Galusková: conceptualization, validation, supervision, writing – review & editing, project administration, and funding acquisition.

Conflicts of interest

There are no conflicts to declare.

Acknowledgements

References

1 H. C. Blair, L. J. Robinson, C. L.-H. Huang, L. Sun, P. A. Friedman, P. H. Schlesinger and M. Zaidi, Calcium and bone disease, *BioFactors*, 2011, **37**, 159–167, DOI: **10.1002/biof.143**.

2 B. L. Foster, K. A. Tompkins, R. B. Rutherford, H. Zhang, E. Y. Chu, H. Fong and M. J. Somerman, Phosphate: known and potential roles during development and regeneration of teeth and supporting structures, *Birth Defects Res., Part C*, 2008, **84**, 281–314, DOI: **10.1002/bdrc.20136**.

3 S. Gomez, R. Rizzo, M. Pozzi-Mucelli, E. Bonucci and F. Vittur, Zinc mapping in bone tissues by histochemistry and synchrotron radiation–induced x-ray emission: correlation with the distribution of alkaline phosphatase, *Bone*, 1999, **25**, 33–38, DOI: **10.1016/S8756-3282(99)00102-7**.

4 H. G. Classen, S. Baier, H. F. Schimatschek and C. U. Classen, Clinically Relevant Interactions between Hormones and Magnesium Metabolism – A Review, *Magnesium-Bulletin B*, 1995, **17**, 96–103.

5 J. Y. Reginster, E. Seeman, M. C. de Vernejoul, S. Adami, J. Compston, C. Phenekos, J. P. Devogelaer, M. D. Curiel, A. Sawicki, S. Goemaere, O. H. Sorensen, D. Felsenberg and P. J. Meunier, Strontium Ranelate Reduces the Risk of Nonvertebral Fractures in Postmenopausal Women with Osteoporosis: Treatment of Peripheral Osteoporosis (TRO-POS) Study, *J. Clin. Endocrinol. Metab.*, 2005, **90**, 2816–2822, DOI: **10.1210/jc.2004-1774**.

6 H. Siddiqui, K. Pickering and M. Mucalo, A Review on the Use of Hydroxyapatite-Carbonaceous Structure Composites in Bone Replacement Materials for Strengthening Purposes, *Materials*, 2018, **11**, 1813, DOI: **10.3390/ma11101813**.

7 V. Lalzawmliana, A. Anand, V. Kumar, P. Das, K. B. Devi, J. Mukherjee, A. K. Maji, B. Kundu, M. Roy and S. K. Nandi, Potential of growth factor incorporated mesoporous bioactive glass for in vivo bone regeneration, *J. Mech. Behav. Biomed. Mater.*, 2019, **91**, 182–192, DOI: **10.1016/j.jmbbm.2018.12.012**.

8 V. Lalzawmliana, A. Anand, M. Roy, B. Kundu and S. K. Nandi, Mesoporous bioactive glasses for bone healing and biomolecules delivery, *Mater. Sci. Eng., C*, 2020, **106**, 110180, DOI: **10.1016/j.msec.2019.110180**.

9 A. Anand, V. Lalzawmliana, V. Kumar, P. Das, K. B. Devi, A. K. Maji, B. Kundu, M. Roy and S. K. Nandi, Preparation and in vivo biocompatibility studies of different mesoporous bioactive glasses, *J. Mech. Behav. Biomed. Mater.*, 2019, **89**, 89–98, DOI: **10.1016/j.jmbbm.2018.09.024**.

10 I. Izquierdo-Barba and M. Vallet-Regí, Mesoporous bioactive glasses: relevance of their porous structure compared to that of classical bioglasses, *Biomed. Glasses*, 2015, **1**, 140–150, DOI: **10.1515/bglass-2015-0014**.

11 C. Wu, Y. Zhou, C. Lin, J. Chang and Y. Xiao, Strontium-containing mesoporous bioactive glass scaffolds with improved osteogenic/cementogenic differentiation of periodontal ligament cells for periodontal tissue engineering, *Acta Biomater.*, 2012, **8**, 3805–3815, DOI: **10.1016/j.actbio.2012.06.023**.

12 J. H. Beattie and A. Avenell, Trace Element Nutrition and Bone Metabolism, *Nutr. Res. Rev.*, 1992, **5**, 167–188, DOI: **10.1079/NRR19920013**.

13 A. Hoppe, N. S. Güldal and A. R. Boccaccini, A review of the biological response to ionic dissolution products from bioactive glasses and glass-ceramics, *Biomaterials*, 2011, **32**, 2757–2774, DOI: **10.1016/j.biomaterials.2011.01.004**.

14 C. Gérard, L.-J. Bordeleau, J. Barralet and C. J. Doillon, The stimulation of angiogenesis and collagen deposition by copper, *Biomaterials*, 2010, **31**, 824–831, DOI: **10.1016/j.biomaterials.2009.10.009**.

15 V. Stanić, S. Dimitrijević, J. Antić-Stanković, M. Mitrić, B. Jokić, I. B. Plećaš and S. Raičević, Synthesis, characterization and antimicrobial activity of copper and zinc-doped hydroxyapatite nanopowders, *Appl. Surf. Sci.*, 2010, **256**, 6083–6089, DOI: **10.1016/j.apsusc.2010.03.124**.

16 J. P. Ruparelia, A. K. Chatterjee, S. P. Duttagupta and S. Mukherji, Strain specificity in antimicrobial activity of silver and copper nanoparticles, *Acta Biomater.*, 2008, **4**, 707–716, DOI: **10.1016/j.actbio.2007.11.006**.

17 K.-Y. Yoon, J. Hoon Byeon, J.-H. Park and J. Hwang, Susceptibility constants of Escherichia coli and Bacillus subtilis to silver and copper nanoparticles, *Sci. Total Environ.*, 2007, **373**, 572–575, DOI: **10.1016/j.scitotenv.2006.11.007**.

18 C. Wu, Y. Zhou, M. Xu, P. Han, L. Chen, J. Chang and Y. Xiao, Copper-containing mesoporous bioactive glass scaffolds with multifunctional properties of angiogenesis capacity, osteo-stimulation and antibacterial activity, *Biomaterials*, 2013, **34**, 422–433, DOI: **10.1016/j.biomaterials.2012.09.066**.

19 L. B. Romero-Sánchez, M. Marí-Beffa, P. Carrillo, M. Á. Medina and A. Díaz-Cuenca, Copper-containing mesoporous bioactive glass promotes angiogenesis in an in vivo

1888 | *J. Mater. Chem. B*, 2024, **12**, 1875–1891

This journal is © The Royal Society of Chemistry 2024

zebrafish model, *Acta Biomater.*, 2018, **68**, 272–285, DOI: 10.1016/j.actbio.2017.12.032.

20 H. Zreiqat, C. R. Howlett, A. Zannettino, P. Evans, G. Schulze-Tanzil, C. Knabe and M. Shakibaei, Mechanisms of magnesium-stimulated adhesion of osteoblastic cells to commonly used orthopaedic implants, *J. Biomed. Mater. Res.*, 2002, **62**, 175–184, DOI: 10.1002/jbm.10270.

21 Y. Yamasaki, Y. Yoshida, M. Okazaki, A. Shimazu, T. Uchida, T. Kubo, Y. Akagawa, Y. Hamada, J. Takahashi and N. Matsuura, Synthesis of functionally graded $MgCO_3$ apatite accelerating osteoblast adhesion, *J. Biomed. Mater. Res.*, 2002, **62**, 99–105, DOI: 10.1002/jbm.10220.

22 M. Shoaib, A. Bahadur, S. Iqbal, M. M. AL-Anazy, A. Laref, M. A. Tahir, P. A. Channar, S. Noreen, M. Yasir, A. Iqbal and K. W. Ali, Magnesium doped mesoporous bioactive glass nanoparticles: a promising material for apatite formation and mitomycin c delivery to the MG-63 cancer cells, *J. Alloys Compd.*, 2021, **866**, 159013, DOI: 10.1016/j.jallcom.2021.159013.

23 S. Sánchez-Salcedo, A. García, A. González-Jiménez and M. Vallet-Regí, Antibacterial effect of 3D printed mesoporous bioactive glass scaffolds doped with metallic silver nanoparticles, *Acta Biomater.*, 2023, **155**, 654–666, DOI: 10.1016/j.actbio.2022.10.045.

24 A. El-Fiqi and H.-W. Kim, Sol–gel synthesis and characterization of novel cobalt ions-containing mesoporous bioactive glass nanospheres as hypoxia and ferroptosis-inducing nanotherapeutics, *J. Non-Cryst. Solids*, 2021, **569**, 120999, DOI: 10.1016/j.jnoncrysol.2021.120999.

25 S. Mortazavi, M. Rahsepar and S. Hosseinzadeh, Modification of mesoporous structure of silver-doped bioactive glass with antibacterial properties for bone tissue applications, *Ceram. Int.*, 2022, **48**, 8276–8285, DOI: 10.1016/j.ceramint.2021.12.032.

26 I. Atkinson, E. M. Anghel, L. Predoana, O. C. Mocioiu, L. Jecu, I. Raut, C. Munteanu, D. Culita and M. Zaharescu, Influence of ZnO addition on the structural, in vitro behavior and antimicrobial activity of sol–gel derived $CaO–P_2O_5–SiO_2$ bioactive glasses, *Ceram. Int.*, 2016, **42**, 3033–3045, DOI: 10.1016/j.ceramint.2015.10.090.

27 C. Wu, Y. Zhou, M. Xu, P. Han, L. Chen, J. Chang and Y. Xiao, Copper-containing mesoporous bioactive glass scaffolds with multifunctional properties of angiogenesis capacity, osteostimulation and antibacterial activity, *Biomaterials*, 2013, **34**, 422–433, DOI: 10.1016/j.biomaterials.2012.09.066.

28 L. B. Romero-Sánchez, M. Marí-Beffa, P. Carrillo, M. Á. Medina and A. Díaz-Cuenca, Copper-containing mesoporous bioactive glass promotes angiogenesis in an in vivo zebrafish model, *Acta Biomater.*, 2018, **68**, 272–285, DOI: 10.1016/j.actbio.2017.12.032.

29 C. Wu, Y. Zhou, C. Lin, J. Chang and Y. Xiao, Strontium-containing mesoporous bioactive glass scaffolds with improved osteogenic/cementogenic differentiation of periodontal ligament cells for periodontal tissue engineering, *Acta Biomater.*, 2012, **8**, 3805–3815, DOI: 10.1016/j.actbio.2012.06.023.

30 Z. Tabia, K. El Mabrouk, M. Bricha and K. Nouneh, Mesoporous bioactive glass nanoparticles doped with magnesium:

drug delivery and acellular in vitro bioactivity, *RSC Adv.*, 2019, **9**, 12232–12246, DOI: 10.1039/C9RA01133A.

31 M. Shoaib, A. Bahadur, S. Iqbal, M. M. AL-Anazy, A. Laref, M. A. Tahir, P. A. Channar, S. Noreen, M. Yasir, A. Iqbal and K. W. Ali, Magnesium doped mesoporous bioactive glass nanoparticles: a promising material for apatite formation and mitomycin c delivery to the MG-63 cancer cells, *J. Alloys Compd.*, 2021, **866**, 159013, DOI: 10.1016/j.jallcom.2021.159013.

32 F. Kermani, S. Mollazadeh Beidokhti, F. Baino, Z. Gholamzadeh-Virany, M. Mozafari and S. Kargozar, Strontium- and Cobalt-Doped Multicomponent Mesoporous Bioactive Glasses (MBGs) for Potential Use in Bone Tissue Engineering Applications, *Materials*, 2020, **13**, 1348, DOI: 10.3390/ma13061348.

33 P. Balasubramanian, A. J. Salinas, S. Sanchez-Salcedo, R. Detsch, M. Vallet-Regi and A. R. Boccaccini, Induction of VEGF secretion from bone marrow stromal cell line (ST-2) by the dissolution products of mesoporous silica glass particles containing CuO and SrO, *J. Non-Cryst. Solids*, 2018, **500**, 217–224, DOI: 10.1016/j.jnoncrysol.2018.07.073.

34 A. Moghanian, A. Ghorbanoghli, M. Kazem-Rostami, A. Pazhouheshgar, E. Salari, M. Saghafi Yazdi, T. Alimardani, H. Jahani, F. Sharifian Jazi and M. Tahriri, Novel antibacterial Cu/Mg-substituted 58S-bioglass: synthesis, characterization and investigation of in vitro bioactivity, *Int. J. Appl. Glass Sci.*, 2020, **11**, 685–698, DOI: 10.1111/ijag.14510.

35 I. Cacciotti, M. Lombardi, A. Bianco, A. Ravaglioli and L. Montanaro, Sol–gel derived 45S5 bioglass: synthesis, microstructural evolution and thermal behaviour, *J. Mater. Sci.: Mater. Med.*, 2012, **23**, 1849–1866, DOI: 10.1007/s10856-012-4667-6.

36 T. Anh Tuan, E. V. Guseva, N. Anh Tien, H. Tan Dat and B. X. Vuong, Simple and Acid-Free Hydrothermal Synthesis of Bioactive Glass $58SiO_2–33CaO–9P_2O_5$ (wt%), *Crystals*, 2021, **11**, 283, DOI: 10.3390/cryst11030283.

37 A. Anand, S. Sengupta, H. Kaňková, A. Švančárková, A. M. Beltrán, D. Galusek, A. R. Boccaccini and D. Galusková, Influence of Copper-Strontium Co-Doping on Bioactivity, Cytotoxicity and Antibacterial Activity of Mesoporous Bioactive Glass, *Gels*, 2022, **8**, 743, DOI: 10.3390/gels8110743.

38 N. Pajares-Chamorro and X. Chatzistavrou, Bioactive Glass Nanoparticles for Tissue Regeneration, *ACS Omega*, 2020, **5**, 12716–12726, DOI: 10.1021/acsomega.0c00180.

39 K. Zheng, N. Taccardi, A. M. Beltrán, B. Sui, T. Zhou, V. R. R. Marthala, M. Hartmann and A. R. Boccaccini, Timing of calcium nitrate addition affects morphology, dispersity and composition of bioactive glass nanoparticles, *RSC Adv.*, 2016, **6**, 95101–95111, DOI: 10.1039/C6RA05548F.

40 J. Chen, L. Zeng, X. Chen, T. Liao and J. Zheng, Preparation and characterization of bioactive glass tablets and evaluation of bioactivity and cytotoxicity in vitro, *Bioact. Mater.*, 2018, **3**, 315–321, DOI: 10.1016/j.bioactmat.2017.11.004.

41 A. López-Noriega, D. Arcos, I. Izquierdo-Barba, Y. Sakamoto, O. Terasaki and M. Vallet-Regí, Ordered Mesoporous Bioactive Glasses for Bone Tissue Regeneration, *Chem. Mater.*, 2006, **18**, 3137–3144, DOI: 10.1021/cm060480o.

This journal is © The Royal Society of Chemistry 2024

J. Mater. Chem. B, 2024, **12**, 1875–1891 | **1889**

42 T. Kimura, Evaporation-induced Self-assembly Process Controlled for Obtaining Highly Ordered Mesoporous Materials with Demanded Morphologies, *Chem. Rec.*, 2016, **16**, 445–457, DOI: **10.1002/tcr.201500262**.

43 L. Sierra, S. Valange, J. Barrault and J.-L. Guth, Templating behavior of a triblock copolymer surfactant with very long hydrophilic PEO chains (PEO140PPO39PEO140) for the synthesis of cubic mesoporous silica with large cage-like cavities, *Microporous Mesoporous Mater.*, 2008, **113**, 352–361, DOI: **10.1016/j.micromeso.2007.11.033**.

44 L. L. Hench and J. M. Polak, Third-Generation Biomedical Materials, *Science*, 1979, **295**(2002), 1014–1017, DOI: **10.1126/science.1067404**.

45 C. Wu, J. Chang and Y. Xiao, Mesoporous bioactive glasses as drug delivery and bone tissue regeneration platforms, *Ther. Deliv.*, 2011, **2**, 1189–1198, DOI: **10.4155/tde.11.84**.

46 D. S. Brauer, Bioactive Glasses-Structure and Properties, *Angew. Chem., Int. Ed.*, 2015, **54**, 4160–4181, DOI: **10.1002/anie.201405310**.

47 X. Yan, X. Huang, C. Yu, H. Deng, Y. Wang, Z. Zhang, S. Qiao, G. Lu and D. Zhao, The in vitro bioactivity of mesoporous bioactive glasses, *Biomaterials*, 2006, **27**, 3396–3403, DOI: **10.1016/j.biomaterials.2006.01.043**.

48 S. Kapoor, A. Goel, A. Tilocca, V. Dhuna, G. Bhatia, K. Dhuna and J. M. F. Ferreira, Role of glass structure in defining the chemical dissolution behavior, bioactivity and antioxidant properties of zinc and strontium co-doped alkali-free phosphosilicate glasses, *Acta Biomater.*, 2014, **10**, 3264–3278, DOI: **10.1016/j.actbio.2014.03.033**.

49 J. R. Jones, P. Sepulveda and L. L. Hench, Dose-dependent behavior of bioactive glass dissolution, *J. Biomed. Mater. Res.*, 2001, **58**, 720–726, DOI: **10.1002/jbm.10053**.

50 D. Huang, K. Ma, X. Cai, X. Yang, Y. Hu, P. Huang, F. Wang, T. Jiang and Y. Wang, Evaluation of antibacterial, angiogenic, and osteogenic activities of green synthesized gap-bridging copper-doped nanocomposite coatings, *Int. J. Nanomed.*, 2017, **12**, 7483–7500, DOI: **10.2147/IJN.S141272**.

51 N. Kong, K. Lin, H. Li and J. Chang, Synergy effects of copper and silicon ions on stimulation of vascularization by copper-doped calcium silicate, *J. Mater. Chem. B*, 2014, **2**, 1100–1110, DOI: **10.1039/C3TB21529F**.

52 H. Wang, S. Zhao, J. Zhou, Y. Shen, W. Huang, C. Zhang, M. N. Rahaman and D. Wang, Evaluation of borate bioactive glass scaffolds as a controlled delivery system for copper ions in stimulating osteogenesis and angiogenesis in bone healing, *J. Mater. Chem. B*, 2014, **2**, 8547–8557, DOI: **10.1039/C4TB01355G**.

53 J. M. Oliveira, R. N. Correia and M. H. Fernandes, Effects of Si speciation on the in vitro bioactivity of glasses, *Biomaterials*, 2002, **23**, 371–379, DOI: **10.1016/S0142-9612(01)00115-6**.

54 E. Dietrich, H. Oudadesse, A. Lucas-Girot and M. Mami, In vitro bioactivity of melt-derived glass 46S6 doped with magnesium, *J. Biomed. Mater. Res., Part A*, 2009, **88A**, 1087–1096, DOI: **10.1002/jbm.a.31901**.

55 J. Chen, L. Zeng, X. Chen, T. Liao and J. Zheng, Preparation and characterization of bioactive glass tablets and evaluation of bioactivity and cytotoxicity in vitro, *Bioact. Mater.*, 2018, **3**, 315–321, DOI: **10.1016/j.bioactmat.2017.11.004**.

56 A. Balamurugan, G. Balossier, S. Kannan, J. Michel, A. H. S. Rebelo and J. M. F. Ferreira, Development and in vitro characterization of sol–gel derived CaO–P₂O₅–SiO₂–ZnO bioglass, *Acta Biomater.*, 2007, **3**, 255–262, DOI: **10.1016/j.actbio.2006.09.005**.

57 F. Baino, Copper-Doped Ordered Mesoporous Bioactive Glass: A Promising Multifunctional Platform for Bone Tissue Engineering, *Bioengineering*, 2020, **7**, 45, DOI: **10.3390/bioengineering7020045**.

58 E. Fiume, C. Migneco, E. Verné and F. Baino, Comparison between Bioactive Sol–Gel and Melt-Derived Glasses/Glass-Ceramics Based on the Multicomponent SiO₂–P₂O₅–CaO–MgO–Na₂O–K₂O System, *Materials*, 2020, **13**, 540, DOI: **10.3390/ma13030540**.

59 C. Pautke, M. Schieker, T. Tischer, A. Kolk, P. Neth, W. Mutschler and S. Milz, Characterization of osteosarcoma cell lines MG-63, Saos-2 and U-2 OS in comparison to human osteoblasts, *Anticancer Res.*, 2004, **24**, 3743–3748.

60 E. M. Czekanska, M. J. Stoddart, J. R. Ralphs, R. G. Richards and J. S. Hayes, A phenotypic comparison of osteoblast cell lines versus human primary osteoblasts for biomaterials testing, *J. Biomed. Mater. Res., Part A*, 2014, **102**, 2636–2643, DOI: **10.1002/jbm.a.34937**.

61 C. Heras, S. Sanchez-Salcedo, D. Lozano, J. Peña, P. Esbrit, M. Vallet-Regi and A. J. Salinas, Osteostatin potentiates the bioactivity of mesoporous glass scaffolds containing Zn²⁺ ions in human mesenchymal stem cells, *Acta Biomater.*, 2019, **89**, 359–371, DOI: **10.1016/j.actbio.2019.03.033**.

62 P. K. Stoimenov, R. L. Klinger, G. L. Marchin and K. J. Klabunde, Metal Oxide Nanoparticles as Bactericidal Agents, *Langmuir*, 2002, **18**, 6679–6686, DOI: **10.1021/la0202374**.

63 M. Raffi, S. Mehrwan, T. M. Bhatti, J. I. Akhter, A. Hameed, W. Yawar and M. M. ul Hasan, Investigations into the antibacterial behavior of copper nanoparticles against Escherichia coli, *Ann. Microbiol.*, 2010, **60**, 75–80, DOI: **10.1007/s13213-010-0015-6**.

64 A. R. Tuttle, N. D. Trahan and M. S. Son, Growth and Maintenance of *Escherichia coli* Laboratory Strains, *Curr. Protoc.*, 2021, **1**, e20, DOI: **10.1002/cpz1.20**.

65 S. Ran, Z. He and J. Liang, Survival of Enterococcus faecalis during alkaline stress: changes in morphology, ultrastructure, physiochemical properties of the cell wall and specific gene transcripts, *Arch. Oral Biol.*, 2013, **58**, 1667–1676, DOI: **10.1016/j.archoralbio.2013.08.013**.

66 T. Pilizota and J. W. Shaevitz, Plasmolysis and Cell Shape Depend on Solute Outer-Membrane Permeability during Hyperosmotic Shock in *E. coli*, *Biophys. J.*, 2013, **104**, 2733–2742, DOI: **10.1016/j.bpj.2013.05.011**.

67 L. Drago, E. De Vecchi, M. Bortolin, M. Toscano, R. Mattina and C. L. Romanò, Antimicrobial activity and resistance selection of different bioglass S53P4 formulations against multidrug resistant strains, *Future Microbiol.*, 2015, **10**, 1293–1299, DOI: **10.2217/FMB.15.57**.

1890 | *J. Mater. Chem. B*, 2024, **12**, 1875–1891

This journal is © The Royal Society of Chemistry 2024

68 L. Drago, M. Toscano and M. Bottagisio, Recent Evidence on Bioactive Glass Antimicrobial and Antibiofilm Activity: A Mini-Review, *Materials*, 2018, **11**, 326, DOI: **10.3390/ma11020326**.

69 C. Ning, X. Wang, L. Li, Y. Zhu, M. Li, P. Yu, L. Zhou, Z. Zhou, J. Chen, G. Tan, Y. Zhang, Y. Wang and C. Mao, Concentration Ranges of Antibacterial Cations for Showing the Highest Antibacterial Efficacy but the Least Cytotoxicity against Mammalian Cells: Implications for a New Antibacterial Mechanism, *Chem. Res. Toxicol.*, 2015, **28**, 1815–1822, DOI: **10.1021/acs.chemrestox.5b00258**.

70 J. Zan, Y. Shuai, J. Zhang, J. Zhao, B. Sun and L. Yang, Hyaluronic acid encapsulated silver metal organic framework for the construction of a slow-controlled bifunctional nanostructure: antibacterial and anti-inflammatory in intrauterine adhesion repair, *Int. J. Biol. Macromol.*, 2023, **230**, 123361, DOI: **10.1016/j.ijbiomac.2023.123361**.

This journal is © The Royal Society of Chemistry 2024

J. Mater. Chem. B, 2024, **12**, 1875–1891 | **1891**